

Article

Non-Covalent Interactions in Hydrogen Storage Materials $\text{LiN}(\text{CH}_3)_2\text{BH}_3$ and $\text{KN}(\text{CH}_3)_2\text{BH}_3$

Filip Sagan, Radosław Filas and Mariusz P. Mitoraj *

Department of Theoretical Chemistry, Faculty of Chemistry, Jagiellonian University, R. Ingardena 3, Cracow 30-060, Poland; filip.sagan@doctoral.uj.edu.pl (F.S.); radoslaw.filas4854@gmail.com (R.F.)

* Correspondence: mitoraj@chemia.uj.edu.pl; Tel.: +48-12-6632042

Academic Editor: Sławomir J. Grabowski

Received: 29 January 2016; Accepted: 14 March 2016; Published: 18 March 2016

Abstract: In the present work, an in-depth, qualitative and quantitative description of non-covalent interactions in the hydrogen storage materials $\text{LiN}(\text{CH}_3)_2\text{BH}_3$ and $\text{KN}(\text{CH}_3)_2\text{BH}_3$ was performed by means of the charge and energy decomposition method (ETS-NOCV) as well as the Interacting Quantum Atoms (IQA) approach. It was determined that both crystals are stabilized by electrostatically dominated intra- and intermolecular $\text{M}\cdots\text{H}-\text{B}$ interactions ($\text{M} = \text{Li}, \text{K}$). For $\text{LiN}(\text{CH}_3)_2\text{BH}_3$ the intramolecular charge transfer appeared ($\text{B}-\text{H}\rightarrow\text{Li}$) to be more pronounced compared with the corresponding intermolecular contribution. We clarified for the first time, based on the ETS-NOCV and IQA methods, that homopolar $\text{BH}\cdots\text{HB}$ interactions in $\text{LiN}(\text{CH}_3)_2\text{BH}_3$ can be considered as destabilizing (due to the dominance of repulsion caused by negatively charged borane units), despite the fact that some charge delocalization within $\text{BH}\cdots\text{HB}$ contacts is enforced (which explains $\text{H}\cdots\text{H}$ bond critical points found from the QTAIM method). Interestingly, quite similar (to $\text{BH}\cdots\text{HB}$) intermolecular homopolar dihydrogen bonds $\text{CH}\cdots\text{HC}$ appeared to significantly stabilize both crystals—the ETS-NOCV scheme allowed us to conclude that $\text{CH}\cdots\text{HC}$ interactions are dispersion dominated, however, the electrostatic and $\sigma/\sigma^*(\text{C}-\text{H})$ charge transfer contributions are also important. These interactions appeared to be more pronounced in $\text{KN}(\text{CH}_3)_2\text{BH}_3$ compared with $\text{LiN}(\text{CH}_3)_2\text{BH}_3$.

Keywords: hydrogen storage materials; non-covalent interactions; dihydrogen bonds; charge and energy decomposition ETS-NOCV

1. Introduction

An increase in energy consumption as well as the environmental harmfulness of current coal or hydrocarbon based fuels has led to intensive search for alternative energy sources [1–3]. Therefore, various hydrogen storage materials, that contain significant amounts of hydrogen, have been recently proposed. Boranes are probably one of the best known group among numerous hydrogen storage materials [4–10]. For example one can present ammonia borane (NH_3BH_3) [4–10]—the attractiveness of this material stems from its high stability, even at higher temperature (the melting point is 104°C), as well as its large hydrogen storage capacity (19.6 wt% H_2). It has been demonstrated that the former feature of ammonia borane crystal originates predominantly from the existence of polar dihydrogen bonds $\text{N}-\text{H}^{\delta+}\cdots-\delta\text{H}-\text{B}$ between monomers [11–16]. Furthermore, it has been proven that the presence of $\text{N}-\text{H}^{\delta+}\cdots-\delta\text{H}-\text{B}$ as well as other non-covalent interactions not only determines the stability, but it can also facilitate various steps of dehydrogenation [5–8,11–23].

It has been shown that incorporation of alkali metals into boranes might accelerate thermolytic dehydrogenation as well as reduce formation of volatile byproducts [24–26]. Therefore various hybrid type materials have also been proposed and extensively studied—as examples one can present $\text{LiBH}_4/\text{NH}_3\text{BH}_3$ [27], $\text{M}[\text{Zn}(\text{BH}_4)_3]$, $\text{M} = \text{Li}, \text{Na}, \text{K}$ [28] or $\text{Al}(\text{BH}_4)_3\cdot\text{NH}_3\text{BH}_3$ [25].

Quite recently McGrady and coworkers published the cutting-edge article in which they had synthesized and characterized two further hydrogen rich crystals $\text{LiN}(\text{CH}_3)_2\text{BH}_3$ and $\text{KN}(\text{CH}_3)_2\text{BH}_3$ [29]. They are depicted in Figure 1. In addition, the authors performed topological electron density based study by means of the QTAIM method of Bader [30]—it was reported that mainly $\text{M}\cdots\text{H}-\text{B}$ ($\text{M} = \text{Li}, \text{K}$) interactions stabilize the crystals. Remarkably, the authors also emphasized that, apart from the mentioned non-covalent interactions, one observes untypical homopolar dihydrogen interactions of the types $\text{BH}\cdots\text{HB}$ and $\text{CH}\cdots\text{HC}$ which are found to determine the chain-like 1D architecture of $\text{LiN}(\text{CH}_3)_2\text{BH}_3$ and 2D layers in $\text{KN}(\text{CH}_3)_2\text{BH}_3$ crystal [29], Figure 1 and Figure S1. It is noteworthy that these types of connections are intuitively considered as destabilizing due to the lack of electrostatic attraction between hydrogen atoms—homopolar dihydrogen interactions (especially the intramolecular ones) are still a matter of debate in the literature [31–46]. Very recently more and more evidence has been reported in the literature that highlight the stabilizing nature of homopolar dihydrogen interactions [17,21,29,36–46].

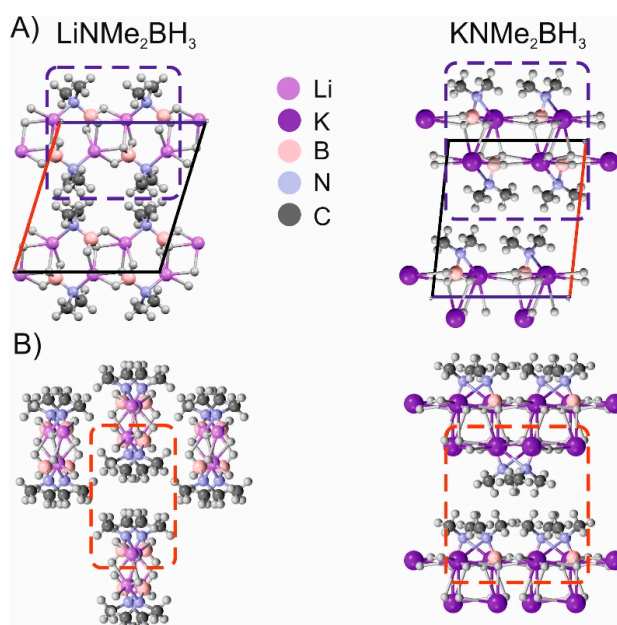


Figure 1. The crystal structures of $\text{LiN}(\text{CH}_3)_2\text{BH}_3$ and $\text{KN}(\text{CH}_3)_2\text{BH}_3$. In addition the cluster models used in the charge and energy decomposition method (ETS-NOCV) analysis are marked by blue (part A) and red dotted lines (part B). The unit cell is also highlighted in the part A.

Accordingly, in this work we provide complementary results which shed light on energetic, quantitative and qualitative characteristics of non-covalent interactions that contribute to the stability of $\text{LiN}(\text{CH}_3)_2\text{BH}_3$ and $\text{KN}(\text{CH}_3)_2\text{BH}_3$ crystals. It is an important goal as it is known that purely topological QTAIM analysis might provide bond paths between atoms (or fragments) even in situations where the overall interaction energies are positive (destabilizing) [36]. Therefore, we applied the charge and energy decomposition scheme (ETS-NOCV) [47–49] which has been proven to provide compact, qualitative and quantitative, descriptions of various types of chemical bonds starting from strong covalent bonds, going through dative connections [47–49] and ending up at various non-covalent interactions [7,8,37,50,51]. We applied the ADF program [52–54] in which the ETS-NOCV scheme is implemented. In order to achieve our goal we chose two types of cluster models—the first type (containing four monomers), marked by a blue dashed line in Figure 1A, is suitable for extraction of $\text{M}\cdots\text{H}-\text{B}$ ($\text{M} = \text{Li}, \text{K}$), and $\text{BH}\cdots\text{HB}$ interactions, whereas the second one (containing eight monomers), depicted by a red dashed line (Figure 1B), contains the $\text{CH}\cdots\text{HC}$ contacts. For selected models we also plotted the reduced density gradient of the NCI (Non-Covalent Index) method [55] in order to

qualitatively characterize non-covalent interactions. In addition, the Interacting Quantum Atoms (IQA) energy decomposition scheme [56] was applied for a quantitative description of selected non-covalent interactions in $\text{LiNMe}_2\text{BH}_3$.

2. Materials and Methods

Our calculations were performed by means of the Amsterdam Density Functional (ADF) program [52–54]. We used DFT/BLYP-D3/TZP because it has been proven many times in the past that they provide satisfactory results for non-covalent interactions [57–59]. The empirical Grimme correction (D3) [60] was used as implemented in the ADF program. We did not calculate basis set superposition errors (BSSE) because these effects are captured in the empirical correction D3 [60]. It is important to emphasize that we also performed additional test calculations for the tetrameric cluster of $\text{LiN}(\text{CH}_3)_2\text{BH}_3$ using the following methods: PBE-D3/TZP, BP86-D3/TZP (ADF program) as well as MP2/6-311 + G**, PBE-D3/6-311 + G**, BP86-D3/6-311 + G**, MO6-2X/6-311 + G**, wB97XD/6-311 + G** (based on the Gaussian package) [61]—the results of total bonding energies appeared to be very similar among all these methods, Tables S1,S2 in ESI file. Accordingly, in the main text we have only discussed the results from ADF/DFT/BLYP-D3/TZP.

In the next paragraph the main formulas of charge and energy decomposition scheme ETS-NOCV are outlined.

2.1. ETS-NOCV

ETS-NOCV method [49] is a merger of the energy decomposition scheme by Ziegler-Rauk [53,62] with the Natural Orbitals for Chemical Valence (NOCV) [47,48].

The natural orbitals for chemical valence (NOCV) are eigenvectors that diagonalize the deformation density matrix:

$$\Delta PC_i = v_i C_i, \Psi_i = \sum_j^N C_{i,j} \lambda_j \quad (1)$$

where C_i is a vector of coefficients, expanding Ψ_i in the basis of fragment orbitals λ_j ; N is a total number of fragment λ_j orbitals. It was shown that the natural orbitals for chemical valence pairs (ψ_{-k}, ψ_k) decompose the differential density $\Delta\rho$ into NOCV-contributions $(\Delta\rho_k)$:

$$\Delta\rho(r) = \sum_{k=1}^{M/2} v_k \left[-\psi_{-k}^2(r) + \psi_k^2(r) \right] = \sum_{k=1}^{M/2} \Delta\rho_k(r) \quad (2)$$

where v_k and M stand for the NOCV eigenvalues and the number of basis functions, respectively. Visual inspection of deformation density plots $(\Delta\rho_k)$ helps to attribute symmetry and the direction of the charge flow. In addition, these pictures are enriched by providing the energetic estimations, $\Delta E_{orb}(k)$, for each $\Delta\rho_k$ within the ETS-NOCV scheme.

The exact formula, which links the ETS and NOCV methods, is given in the next paragraph, after we briefly present the basic concept of the ETS scheme. In this method the *total bonding energy*, ΔE_{total} , between interacting fragments is divided into four components:

$$\Delta E_{total} = \Delta E_{dist} + \Delta E_{elstat} + \Delta E_{Pauli} + \Delta E_{orb} = \Delta E_{dist} + \Delta E_{int} \quad (3)$$

One could add that the negative value $-\Delta E_{total}$ is a bond dissociation energy. The first contribution of Equation (3), ΔE_{dist} , describes the amount of energy required to promote fragments from their equilibrium geometry to the conformations they adopt in the final optimized molecule. The second term, ΔE_{elstat} , corresponds to the classical electrostatic interaction between the promoted fragments as they are brought to their positions in the final complex. The third term, ΔE_{Pauli} , accounts for the repulsive Pauli interaction between occupied orbitals on the two fragments in the combined molecule. Finally, the last stabilizing term, ΔE_{orb} , represents interactions between the occupied molecular orbitals

of one fragment with the unoccupied molecular orbitals of the other fragment as well as mixing of occupied and virtual orbitals within the same fragment (inner-fragment polarization). This energy term is linked to the electronic bonding effect coming from the formation of a chemical bond. In the combined ETS-NOCV scheme [49] the orbital interaction term (ΔE_{orb}) is expressed in terms of NOCV's eigenvalues (v_k) as:

$$\Delta E_{orb} = \sum_k \Delta E_{orb}(k) = \sum_{k=1}^{M/2} v_k \left[-F_{-k,-k}^{TS} + F_{k,k}^{TS} \right] \quad (4)$$

where $F_{i,i}^{TS}$ are diagonal Kohn-Sham matrix elements defined over NOCV with respect to the transition state (TS) density at the midpoint between the density of the molecule and the sum of fragment densities. The above components $\Delta E_{orb}(k)$ provide the energetic estimation of $\Delta\rho_k$ that may be related to the importance of a particular electron flow channel for the bonding between the considered molecular fragments. Finally, in this work we applied a dispersion corrected functional, so this term (ΔE_{disp}) enters additionally into Equation (3). The ETS-NOCV analysis was done based on the Amsterdam Density Functional (ADF) package in which this scheme was implemented.

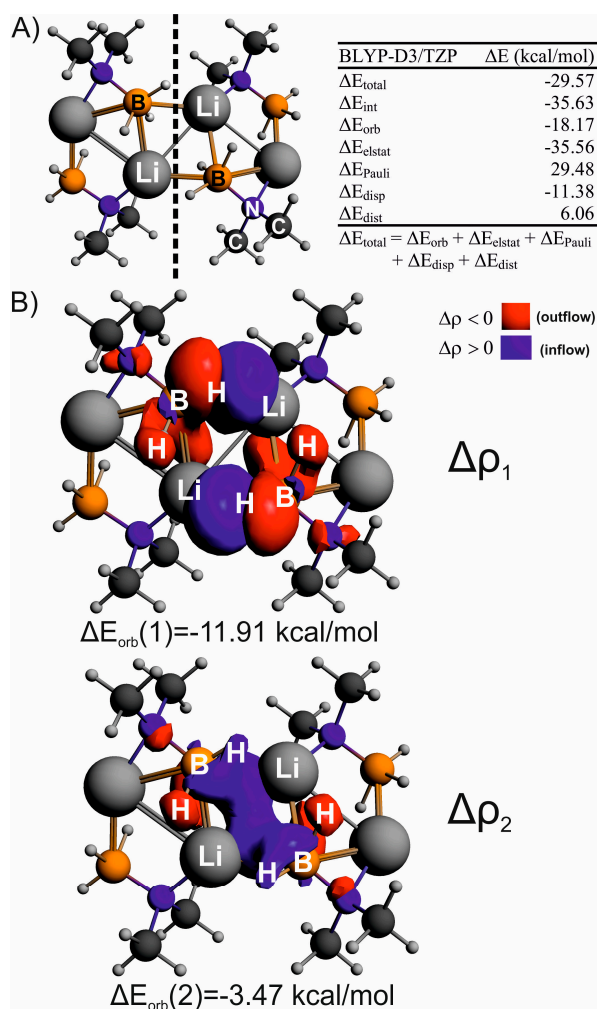


Figure 2. The optimized tetrameric cluster model of $\text{LiN}(\text{CH}_3)_2\text{BH}_3$ along with energy decomposition results describing the interaction between two dimeric fragments in $\text{LiN}(\text{CH}_3)_2\text{BH}_3$ (A). The fragmentation pattern used in ETS-NOCV analysis is indicated by black dashed line. (B) displays the most relevant deformation density contributions describing $\text{Li}\cdots\text{H}-\text{B}$ interactions. The red color of deformation densities shows charge depletion, whereas the blue an electron accumulation due to $\text{Li}\cdots\text{H}-\text{B}$ interaction.

For ETS-NOCV analyses the crystal coordinates (not reoptimized) have been predominantly used in order to reflect the real structures of $\text{LiN}(\text{CH}_3)_2\text{BH}_3$ and $\text{KN}(\text{CH}_3)_2\text{BH}_3$. Accordingly, the distortion energy term, ΔE_{dist} (Equation (3)), was not calculated. Hence, an interaction energy ΔE_{int} was mostly analyzed in this work. We found for the tetrameric lithium model that the reoptimized geometry as well as bonding properties corresponds well to the crystal structure—accordingly, for this system we also considered the ΔE_{dist} term (Figure 2A) and discussed the corresponding total bonding ΔE_{total} and interaction ΔE_{int} energies. It needs to be added that our efforts to reoptimize the remaining models provided geometries which do not correspond to the crystal structures of $\text{LiN}(\text{CH}_3)_2\text{BH}_3$ and $\text{KN}(\text{CH}_3)_2\text{BH}_3$. For monomers the optimized structures are considered for ETS-NOCV analysis as they are similar to crystal geometries—in addition, it allows for discussion of the overall stability of monomers (ΔE_{total} values).

2.2. NCI Technique

It has been shown that the reduced density gradient:

$$s = \frac{1}{2(3\pi^2)^{1/3}} \frac{|\nabla\rho|}{\rho^{4/3}} \quad (5)$$

appeared to be a useful quantity for a description of non-covalent interactions. In order to obtain information about the type of bonding, plot of reduced density gradient s against molecular density ρ is very often examined. When a weak inter- or intramolecular interaction is present, there exists a characteristic spike lying at low values of both density ρ and reduced density gradient s . To distinguish between attractive and repulsive interactions the eigenvalues (λ_i) of the second derivative of density (Hessian, $\nabla^2\rho$) are used, $\nabla^2\rho = \lambda_1 + \lambda_2 + \lambda_3$. Namely, bonding interactions are characterized by $\lambda_2 < 0$, whereas $\lambda_2 > 0$ indicates that the atoms are in non-bonded contact. Therefore, within the NCI technique, one can draw information about non-covalent interactions from the plots of $\text{sign}(\lambda_2)\rho$ vs. s . In such plots the low gradient spike, an indicator of stabilizing interaction, is located within the region of negative values of the density. On the contrary, the repulsive interactions are characterized by positive values of $\text{sign}(\lambda_2)\rho$. One can also plot the contour of s colored by the value of $\text{sign}(\lambda_2)\rho$ providing a pictorial representation of non-covalent interactions.

2.3. IQA (Interacting Quantum Atoms) Energy Decomposition Scheme

The Interacting Quantum Atoms (IQA) approach of Blanco and coworkers [56] allows to partition an electronic energy E into atomic (E_{self}^A) and diatomic contributions ($E_{\text{int}}^{\text{AB}}$):

$$E = \sum_A E_{\text{self}}^A + \frac{1}{2} \sum_A \sum_{B \neq A} E_{\text{int}}^{\text{AB}} \quad (6)$$

The interatomic interaction energy $E_{\text{int}}^{\text{AB}}$ covers all inter-particle interactions: nucleus-nucleus, $V_{\text{nn}}^{\text{AB}}$, nucleus-electron, $V_{\text{ne}}^{\text{AB}}$, electron-nucleus, $V_{\text{en}}^{\text{AB}}$, and electron-electron, $V_{\text{ee}}^{\text{AB}}$, coming from interatomic interaction energies of particles ascribed to atom A with particles ascribed to atom B:

$$E_{\text{int}}^{\text{AB}} = V_{\text{nn}}^{\text{AB}} + V_{\text{en}}^{\text{AB}} + V_{\text{ne}}^{\text{AB}} + V_{\text{ee}}^{\text{AB}} = V_{\text{nn}}^{\text{AB}} + V_{\text{en}}^{\text{AB}} + V_{\text{ne}}^{\text{AB}} + V_{\text{eeC}}^{\text{AB}} + V_{\text{eeX}}^{\text{AB}} \quad (7)$$

The $V_{\text{ee}}^{\text{AB}}$ term can be further divided into exchange ($V_{\text{eeX}}^{\text{AB}}$) and Coulomb ($V_{\text{eeC}}^{\text{AB}}$) contributions. The AIMALL program was used for the IQA calculations [63]. Due to the fact that we are interested in interaction energies in crystals we focused our attention on $E_{\text{int}}^{\text{AB}}$. More details and numerous applications of the IQA technique can be found in Reference [56].

2.4. Molecular Electrostatic Potential (MEP)

The electrostatic potential $V(r)$ of a molecule at point “ r ”, due to nuclei and electrons, is defined as:

$$V(r) = \sum_A \frac{Z_A}{|R_A - r|} - \int \frac{\rho(r')dr'}{|r - r'|} \quad (8)$$

where Z_A is the charge of nucleus at position R_A and $\rho(r)$ is the total electronic density. The sign of $V(r)$ depends upon whether the positive contribution of the nuclei or negative from the electrons is dominant. Negative values of $V(r)$ correspond to nucleophilic areas of the molecule, whereas the positive to electrophilic regions. It has been demonstrated in numerous works that MEP is a very useful quantity for in depth description of electron density distribution [64–67].

3. Results and Discussion

Let us start by discussing factors determining the stability of $\text{LiN}(\text{CH}_3)_2\text{BH}_3$. It can be seen from Figure 2A that the overall interaction energy between fragments, each consisting of the two $\text{LiN}(\text{CH}_3)_2\text{BH}_3$ monomers, is $\Delta E_{\text{int}} = -35.63$ kcal/mol (-17.81 kcal/mol per monomer-monomer interaction). This is in very good agreement with ΔE_{int} obtained for the crystal (non-optimized) geometry, Figure S2. An inclusion of the geometry distortion term leads to an overall bonding energy, $\Delta E_{\text{total}} = -29.57$ kcal/mol. It is noteworthy that other computational protocols provide very similar ΔE_{total} values, Tables S1 and S2.

The dominating contribution (55%) to ΔE_{total} stems from the electrostatic stabilization $\Delta E_{\text{elstat}} = -35.56$ kcal/mol, followed by the orbital interaction $\Delta E_{\text{orb}} = -18.17$ kcal/mol (28%) and the dispersion components $\Delta E_{\text{disp}} = -11.38$ kcal/mol (17%), Figure 2A. The molecular electrostatic potential (MEP) of the monomer demonstrates (Figure 3A) that the borane group is negatively charged, whereas the electrophilic region (positive MEP values) is seen around Li which explains the dominance of the electrostatic term in the intermolecular stabilization of $\text{LiN}(\text{CH}_3)_2\text{BH}_3$.

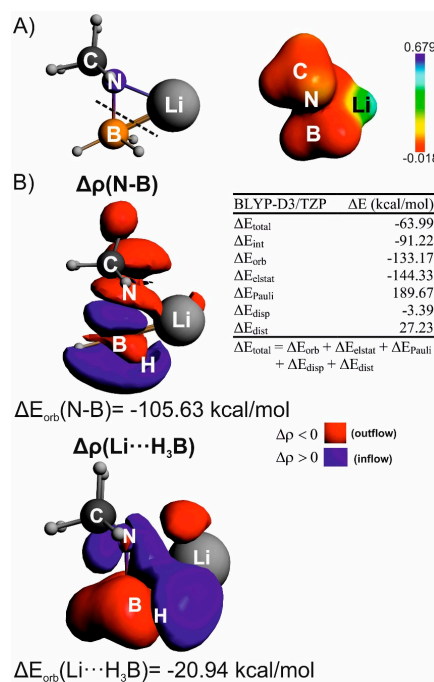


Figure 3. Monomer of $\text{LiN}(\text{CH}_3)_2\text{BH}_3$ along with the corresponding molecular electrostatic potential (A). In (B) the results of ETS-NOCV analysis are presented that describe bonding between the BH_3 unit and the $\text{LiN}(\text{CH}_3)_2$ fragment.

Further decomposition of ΔE_{orb} into deformation density contributions according to the ETS-NOCV scheme is shown in Figure 2B. It can be seen that the leading deformation densities, $\Delta\rho_1$ and $\Delta\rho_2$, depict the formation of $\text{Li}\cdots\text{H}-\text{B}$ bonds. They originate from an outflow of electron density from σ (B–H) bonds to Li^+ ions, Figure 2B, and correspond to the following stabilization, $\Delta E_{\text{orb}}(1) = -11.91$ kcal/mol, $\Delta E_{\text{orb}}(2) = -3.47$ kcal/mol, respectively. Such outflow leads to the elongation of B–H bonds by ~ 0.1 Å (as compared with non-bonding monomers). It is important to emphasize that $\text{Li}\cdots\text{H}-\text{B}$ interactions also lead to some charge delocalization within the “bay” containing two Li ions and two borane units, see $\Delta\rho_2$ in Figure 2B. This is fully consistent with the presence of QTAIM bond critical points between hydrogen atoms in homopolar bridges $\text{BH}\cdots\text{HB}$ as found by McGrady and coworkers [29]. However, an interesting question emerges at this point: is the $\text{LiN}(\text{CH}_3)_2\text{BH}_3$ dimer consisting of two monomers exposed to each other via pure $\text{BH}\cdots\text{HB}$ interaction stable? Such a situation, *i.e.*, the dimer in the geometry of the optimized tetrameric cluster model, is depicted in Figure 4B. Our results clearly indicate that in such a case the overall monomer-monomer interaction energy is positive due to significant Pauli and electrostatic repulsions (with total of $+9.06$ kcal/mol) that overcome subtle stabilization from charge transfer ΔE_{orb} and dispersion ΔE_{disp} (summing up to -4.16 kcal/mol)—accordingly, pure $\text{BH}\cdots\text{HB}$ interactions would destabilize the $\text{LiN}(\text{CH}_3)_2\text{BH}_3$ crystal. The same conclusions are valid when considering the dimer in crystal geometry, Figure S3.

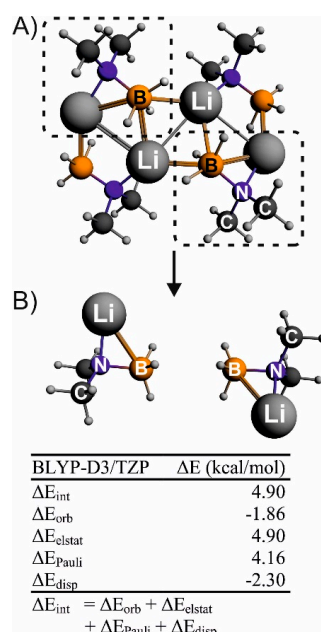


Figure 4. Dimer of $\text{LiN}(\text{CH}_3)_2\text{BH}_3$ consisting of $\text{BH}\cdots\text{HB}$ interactions together with results of ETS-NOCV analysis (B). The dimer was cut from the optimized tetramer model and it is marked with black dotted lines (A).

Furthermore, we have not found any local minimum energy structure on the potential energy surface for a dimer that would contain solely $\text{BH}\cdots\text{HB}$ interaction (a dimer where BH_3 units are exposed to each other). Summarizing, the major stabilization in the $\text{LiN}(\text{CH}_3)_2\text{BH}_3$ crystal arises from electrostatically dominated intermolecular $\text{Li}\cdots\text{H}-\text{B}$ interactions, as previously reported by McGrady *et al.* [29]. The formation of such bonds additionally enforce some charge delocalization within $\text{BH}\cdots\text{HB}$ contacts ($\Delta\rho_2$ in Figure 2B), however, the overall $\text{BH}\cdots\text{HB}$ interaction is destabilizing. Our conclusions are fully in line with the other, mostly experimental studies, in which the destabilizing role of $\text{BH}\cdots\text{HB}$ interactions were also suggested [68–72]. McGrady and coworkers reported the opposite in their series of recent articles [17,20,21,29]. Due to the fact that such interactions are clearly

a matter of debate, in addition, we performed the Interacting Quatum Atoms (IQA) based study for the tetrameric models of $\text{LiNMe}_2\text{BH}_3$. The results are gathered in Table 1.

Table 1. The interacting quatum atoms (IQA) energy decomposition results (in kcal/mol) describing the two atomic interactions $\text{X}\cdots\text{Y}$ ($\text{X}=\text{Li}, \text{H}$; $\text{Y}=\text{H}$) in $\text{LiNMe}_2\text{BH}_3$.

IQA($\text{X}\cdots\text{Y}$)	$V_{\text{ne}}^{\text{AB}}$	$V_{\text{en}}^{\text{AB}}$	$V_{\text{nn}}^{\text{AB}}$	$V_{\text{ee}}^{\text{AB}}$	$V_{\text{eeC}}^{\text{AB}}$	$V_{\text{eeX}}^{\text{AB}}$	$V_{\text{int}}^{\text{AB}*}$
$\text{Li}\cdots\text{H}(\text{B})$	−805.9	−338.4	480.1	565.4	568.2	−2.8	−98.8
$(\text{C})\text{H}\cdots\text{H}(\text{C})$	−140.6	−138.2	130.8	147.2	148.6	−1.4	−0.80
$(\text{B})\text{H}\cdots\text{H}(\text{B})$	−198.9	−198.6	119.7	327.2	330.0	−2.7	+49.4

$$* E_{\text{int}}^{\text{AB}} = V_{\text{nn}}^{\text{AB}} + V_{\text{en}}^{\text{AB}} + V_{\text{ne}}^{\text{AB}} + V_{\text{ee}}^{\text{AB}} = V_{\text{nn}}^{\text{AB}} + V_{\text{en}}^{\text{AB}} + V_{\text{ne}}^{\text{AB}} + V_{\text{eeC}}^{\text{AB}} + V_{\text{eeX}}^{\text{AB}}$$

It is visible from Table 1 that the overall diatomic interaction energies, $E_{\text{int}}^{\text{AB}}$, for $\text{Li}\cdots\text{H}(\text{B})$ and $(\text{C})\text{H}\cdots\text{H}(\text{C})$ are negative, $E_{\text{int}}^{\text{Li}\cdots\text{H}(\text{B})} = -98.8$ kcal/mol, $E_{\text{int}}^{(\text{C})\text{H}\cdots\text{H}(\text{C})} = -0.80$ kcal/mol, which indicates the stabilizing interactions as opposed to the homopolar $(\text{B})\text{H}\cdots\text{H}(\text{B})$ contacts which appeared to be significantly destabilizing, $E_{\text{int}}^{(\text{B})\text{H}\cdots\text{H}(\text{B})} = +49.4$ kcal/mol. This is due to the significantly positive electron-electron repulsion term, $V_{\text{ee}}^{\text{AB}} = 327.2$ kcal/mol, caused in turn by the Coulomb contribution $V_{\text{eeC}}^{\text{AB}} = 330.0$ kcal/mol, Table 1. We also looked at the partial charges in the monomer and tetramer of $\text{LiN}(\text{CH}_3)_2\text{BH}_3$ and found that in both cases the borane units are negatively charged, which conforms to the significant value of the Coulomb repulsion $V_{\text{eeC}}^{\text{AB}}$ found from the IQA analysis, Figure S4 and Table 1. We further calculated the electrostatic interaction between the monomers bonded via $\text{BH}\cdots\text{HB}$ contacts in the presence of the two other monomers (Figure S5). Interestingly, we found the electrostatic repulsion, *ca.* 15.6 kcal/mol, which is even more pronounced than the repulsion noted for the dimer without the neighboring monomers, 7.08 kcal/mol, Figures S3,S5—we determined that it is due to the closely located Li ions which act as electron density attractors making BH_3 units more nucleophilic compared with the monomer, Figure S6. All these results based on the ETS-NOCV, IQA methods, atomic charges and molecular electrostatic potentials allow to conclude on the destabilizing nature of $\text{BH}\cdots\text{HB}$ contacts in $\text{LiN}(\text{CH}_3)_2\text{BH}_3$ —it is important to admit that our results are based on cluster models which might lead to omission of some bonding features in real crystals especially as far as weak non-covalent interactions are taken into account—accordingly, further studies based on other methods within the periodic calculations are necessary in order to fully delineate the nature of homopolar $\text{BH}\cdots\text{HB}$ interactions. Unfortunately, the ETS-NOCV and IQA schemes are not yet available for public use in periodic calculations codes. On the other hand, it seems rational to comment, based on the very huge positive value of the $(\text{B})\text{H}\cdots\text{H}(\text{B})$ interaction energy $E_{\text{int}}^{(\text{B})\text{H}\cdots\text{H}(\text{B})} = +49.4$ kcal/mol in the tetrameric Li-model, that it is to be expected that in the real Li-crystal the $\text{BH}\cdots\text{HB}$ interactions are likely to be destabilizing.

It is probably important to add that the electron density accumulation in the inter-hydrogen region of $\text{BH}\cdots\text{HB}$ is indeed sufficient to observe a bond path (as it has been noted by McGrady *et al.* [29])—however, it does not necessarily imply the overall stabilizing interactions: for example, as nicely demonstrated by Cukrowski *et al.* [36], two water molecules enforced to approach each other via oxygen atoms leads to formation of the oxygen-oxygen bond critical point, however, the overall binding energy is as expected positive (destabilizing) due to the fact that some subtle stabilization arising from the electron-exchange channel (resulting also in the negative ΔE_{orb} values) is diminished by the Pauli and electrostatic repulsion. A similar situation is observed in dimers of M_2X_2 (for $\text{M} = \text{Li}, \text{K}$, $\text{X} = \text{H}, \text{Cl}$) where M-X stabilization outweighs the repulsion stemming from M-M and X-X interactions [73].

In Figure 3A the structure of the $\text{LiN}(\text{CH}_3)_2\text{BH}_3$ monomer is presented. It can be seen that lithium ion forms a chemical bond not only with the nitrogen atom, but also with the BH_3 unit through intramolecular $\text{Li}\cdots\text{H-B}$ interactions. The binding energy of BH_3 to NMe_2Li appears to be significant, $\Delta E_{\text{total}} = -63.99$ kcal/mol, Figure 3B. Just for comparison, the binding energy of BH_3 to ammonia in NH_3BH_3 is only -30.3 kcal/mol [13]. Such a difference is related to the existence of

strong intramolecular Li···H–B interactions. ETS-NOCV allowed us to conclude that, apart from strong dative bonds, described by $\Delta\rho(\text{N-B})$ and the corresponding $\Delta E_{\text{orb}}(\text{B-N}) = -105.63$ kcal/mol, additional intramolecular Li···H–B interactions are formed, $\Delta\rho(\text{Li}\cdots\text{H-B})$. The latter component corresponds to significant charge transfer stabilization, $\Delta E_{\text{orb}}(\text{Li}\cdots\text{H-B}) = -20.94$ kcal/mol, Figure 3B. It is noteworthy that the intramolecular Li···H–B charge transfer component (Figure 3B) appears to be stronger than the intermolecular one, $\Delta E_{\text{orb}}(\text{Li}\cdots\text{H-B}) = -15.38$ kcal/mol (Figure 2B)—this is related to the fact that in the latter case B–H bonds interact with the single Li ion, whereas in the former one with multiple Li ions.

We further performed similar calculations for the tetrameric model of $\text{KN}(\text{CH}_3)_2\text{BH}_3$ as well as for the monomer—the results of ETS-NOCV calculations are shown in Figures 5 and 6. Similarly to $\text{LiN}(\text{CH}_3)_2\text{BH}_3$, intermolecular interactions in the tetramer of $\text{KN}(\text{CH}_3)_2\text{BH}_3$ are dominated by electrostatic forces (60% of total stabilizing contributions), followed by dispersion (22%) and orbital interaction components (18%), Figure 5. The overall intermolecular K···H–B interaction energy is slightly less pronounced compared to the corresponding Li···H–B due to the larger size of potassium compared to lithium. One should point out the lack of BH···HB electron delocalization within the “bay” between the two potassium atoms and BH₃ groups, which is present in $\text{LiN}(\text{CH}_3)_2\text{BH}_3$ ($\Delta\rho_2$ in Figure 2b). It has been already noted by McGrady and coworkers [29]. The B–N dative bond in $\text{KN}(\text{CH}_3)_2\text{BH}_3$ monomer is of similar strength $\Delta E_{\text{orb}}(\text{B-N}) = -104.30$ kcal/mol with respect to $\text{LiN}(\text{CH}_3)_2\text{BH}_3$. The intramolecular K···H–B charge delocalization is of similar magnitude to the intermolecular-one, Figures 5B and 6B. Finally, the overall bonding energy of BH₃ to $\text{KN}(\text{CH}_3)_2$ in the monomer, $\Delta E_{\text{total}} = -67.34$ kcal/mol, appeared to be more negative compared to the corresponding $\Delta E_{\text{total}} = -63.99$ kcal/mol for $\text{LiN}(\text{CH}_3)_2\text{BH}_3$ predominantly due to a lower Pauli repulsion contribution, Figures 3 and 6.

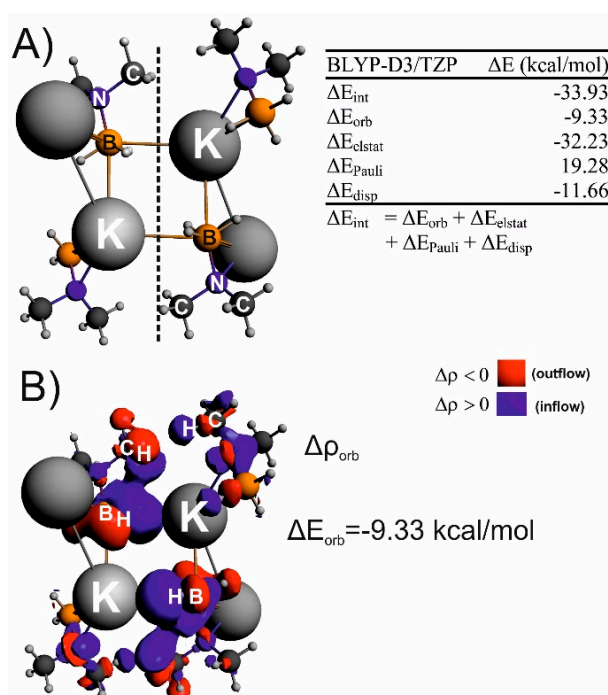


Figure 5. The tetrameric cluster model of $\text{KN}(\text{CH}_3)_2\text{BH}_3$ along with energy decomposition results describing the interaction between two dimeric fragments in $\text{KN}(\text{CH}_3)_2\text{BH}_3$ (A). The fragmentation pattern used in ETS-NOCV analysis is indicated by a black line. Part (B) displays the most relevant deformation density contributions describing K···H–B interactions. The red color of the deformation densities shows charge depletion, whereas the blue an electron accumulation due to K···H–B interaction.

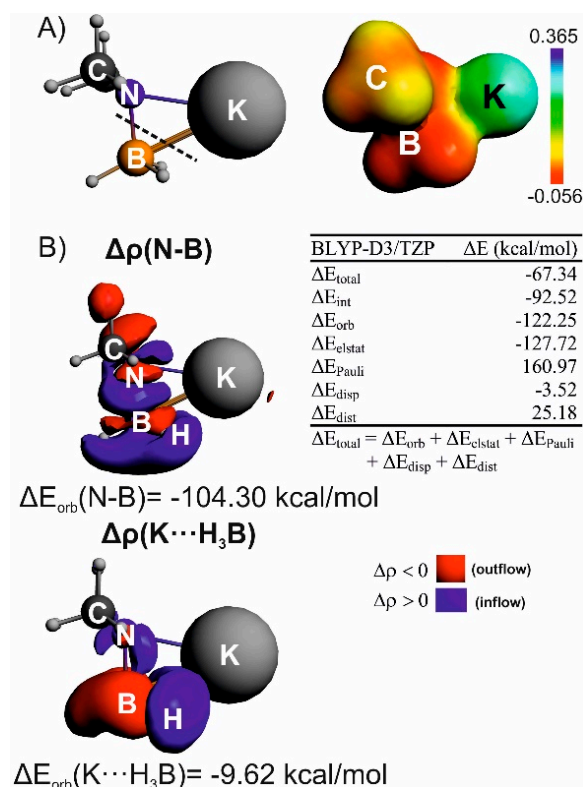


Figure 6. Monomer of $\text{KN}(\text{CH}_3)_2\text{BH}_3$ along with the corresponding molecular electrostatic potential (part (A)). In part (B) the results of ETS-NOCV analysis are presented that describe bonding between the BH_3 unit and the NKMe_2 fragment.

Finally, we consider the two remaining cluster models of $\text{LiN}(\text{CH}_3)_2\text{BH}_3$ and $\text{KN}(\text{CH}_3)_2\text{BH}_3$ where homopolar $\text{CH}\cdots\text{HC}$ interactions are involved, Figures 1B, 7A and 8A.

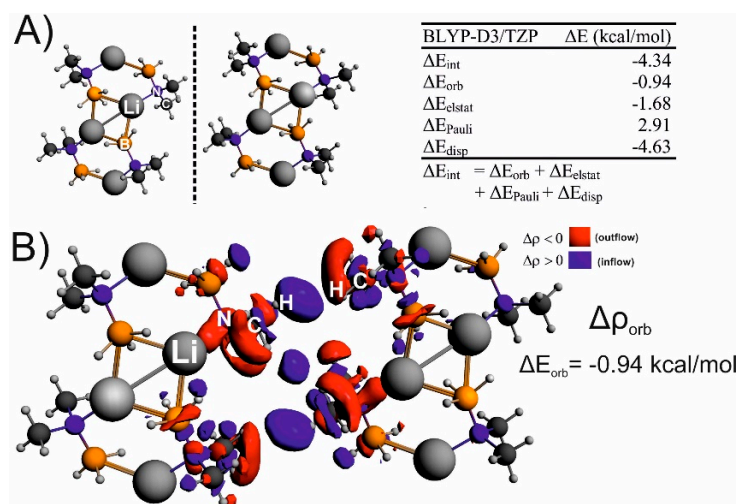


Figure 7. Cluster model containing eight monomers of $\text{LiN}(\text{CH}_3)_2\text{BH}_3$ along with energy decomposition results describing $\text{CH}\cdots\text{HC}$ interactions between the two selected fragments (marked by the black line), part (A). In part (B) the overall deformation density $\Delta\rho_{\text{orb}}$ is depicted together with the corresponding stabilization ΔE_{orb} .

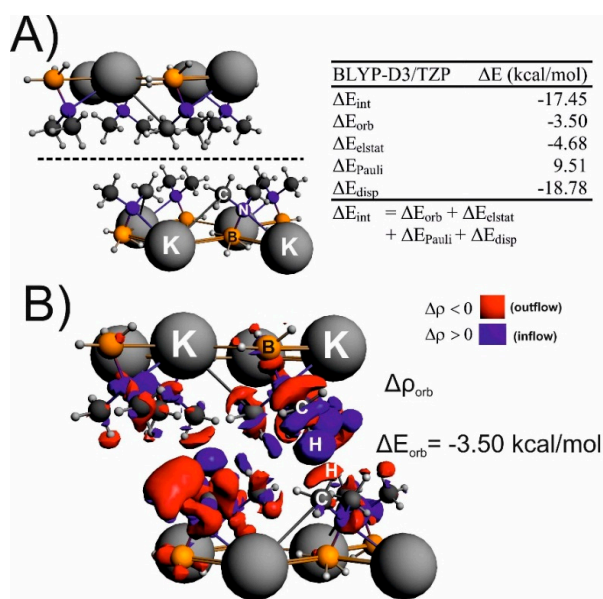


Figure 8. Cluster model containing eight monomers of $\text{KN}(\text{CH}_3)_2\text{BH}_3$ along with energy decomposition results describing $\text{CH}\cdots\text{HC}$ interactions between the two selected fragments (marked by the black line), part (A). In part (B) the overall deformation density $\Delta\rho_{\text{orb}}$ is depicted together with the corresponding stabilization ΔE_{orb} .

The results of energy decomposition analyses demonstrate the stabilizing nature of $\text{CH}\cdots\text{HC}$ interactions in both crystals—the overall interaction energy is $\Delta E_{\text{int}} = -17.45$ kcal/mol for $\text{KN}(\text{CH}_3)_2\text{BH}_3$, whereas it is only $\Delta E_{\text{int}} = -4.34$ kcal/mol for $\text{LiN}(\text{CH}_3)_2\text{BH}_3$, Figures 7A and 8A. Significantly more pronounced stabilization in potassium crystal originates from larger number of $\text{CH}\cdots\text{HC}$ contacts as compared to the lithium analog. It constitutes the 2D layers architecture of the potassium crystal as compared to rather 1D chain-like structure in $\text{LiN}(\text{CH}_3)_2\text{BH}_3$. In both cases the main contribution (64%–68%) to overall stabilization is dispersion, $\Delta E_{\text{disp}} = -4.63$ kcal/mol for $\text{LiN}(\text{CH}_3)_2\text{BH}_3$ and $\Delta E_{\text{disp}} = -18.78$ kcal/mol for $\text{KN}(\text{CH}_3)_2\text{BH}_3$, Figures 7A and 8A. The same has been already suggested by McGrady and coworkers [29]. We found in addition that the electrostatic ΔE_{elstat} and orbital interaction ΔE_{orb} terms are also important, Figures 7A and 8A. Figures 7B and 8B shows that the formation of the $\text{CH}\cdots\text{HC}$ interactions is accompanied by a charge outflow from the occupied $\sigma(\text{C}-\text{H})$ bonds and the electron density accumulation is visible in the inter-hydrogen region of $\text{CH}\cdots\text{HC}$ units. Considering the classical language of a molecular orbital theory one can summarize that the “electronic” part of the $\text{CH}\cdots\text{HC}$ bonding is based on both donation from the occupied $\sigma(\text{C}-\text{H})$ bonds into the empty $\sigma^*(\text{C}-\text{H})$ of methyl groups as well as polarization of the C–H bonds (mixing of $\sigma/\sigma^*(\text{C}-\text{H})$). These stabilizing contributions (the polarization and charge transfer) are clearly mixed—at this point one can reference other important and interesting works in which the meaning of both contributions is debated in terms of non-covalent interactions [67,68,74–76].

It is important to reference other works where dispersion dominated $\text{CH}\cdots\text{HC}$ interactions have been found—Echeverría and coworkers found, based on MP2 studies, the “subtle but not faint” stabilizing $\text{CH}\cdots\text{HC}$ interactions between alkanes [77]. Further Valence Bond studies have revealed [78], in line with our conclusions, that, apart from the crucial dispersion term, also the $\sigma/\sigma^*(\text{C}-\text{H})$ polarization/charge transfer and electrostatic contributions are important. Recently, numerous reports are present in the literature on the stabilizing nature of $\text{CH}\cdots\text{HC}$ interactions in various types of hydrocarbons [37,38,79–85], as well as their importance in catalysis [42,43,86].

In order to complement and confirm the conclusions obtained by the ETS-NOCV method we additionally plotted the contour of the reduced density gradient of the NCI (Non-Covalent Index) method [55] for $\text{KN}(\text{CH}_3)_2\text{BH}_3$, Figure 9. It was demonstrated that this method is well suited for

visualization of non-covalent interactions [55]. It is clearly seen, in line with ETS-NOCV based study, that the crystal of $\text{KN}(\text{CH}_3)_2\text{BH}_3$ is stabilized by numerous inter and intramolecular $\text{K}\cdots\text{H}-\text{B}$ as well as additionally by $\text{CH}\cdots\text{HC}$ interactions. The same is valid for $\text{LiN}(\text{CH}_3)_2\text{BH}_3$. It is to be anticipated that the existence of strong $\text{M}\cdots\text{H}-\text{B}$ interactions in both crystals might affect the mechanism of dehydrogenation similarly as has been already shown for the parent compound LiNH_2BH_3 for which dehydrogenation is initiated by $\text{Li}\cdots\text{H}-\text{B}$ interactions and proceeds further through formation of LiH hydride and NH_2BH_2 as intermediates [87–89].

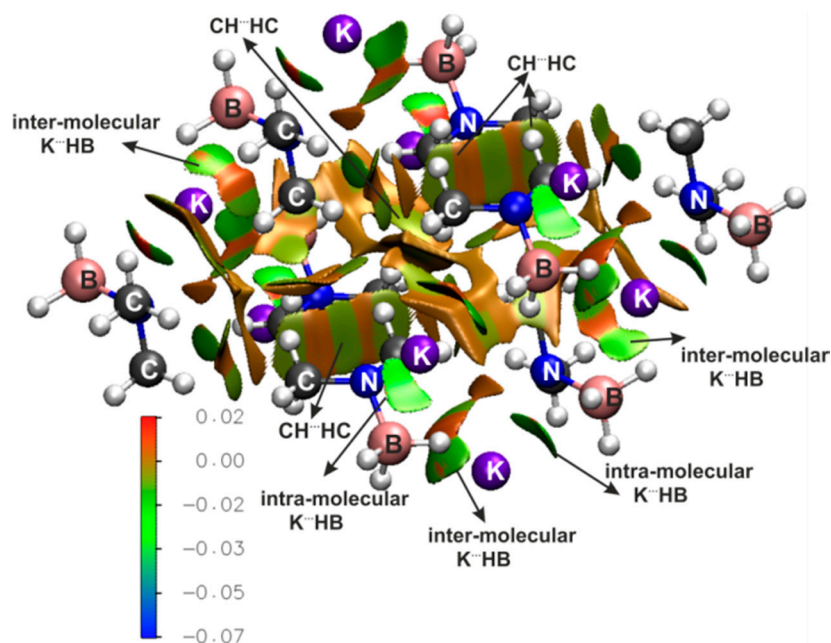


Figure 9. The surfaces describing the reduced density gradient at an isovalue of 0.5 a.u. for the octamer of $\text{KN}(\text{CH}_3)_2\text{BH}_3$. The surfaces are coloured on a blue-green-red scale according to the values of $\text{sign}(\lambda_2)\rho$, ranging from -0.05 to 0.02 au.

4. Conclusions

In the present study non-covalent interactions in the hydrogen storage materials $\text{LiN}(\text{CH}_3)_2\text{BH}_3$ and $\text{KN}(\text{CH}_3)_2\text{BH}_3$ are for the first time quantitatively (and qualitatively) described by means of the charge and energy decomposition method ETS-NOCV as well as the Interacting Quantum Atoms (IQA) approach.

It was found, in line with the pioneering work of McGrady *et al.* [29], that both crystals are stabilized by numerous intra- and intermolecular $\text{M}\cdots\text{H}-\text{B}$ interactions ($\text{M} = \text{Li}, \text{K}$). The ETS-NOCV calculations indicated that these bonds are electrostatically dominated, followed by charge transfer and dispersion contributions. Interestingly, the intramolecular charge transfer contributing to $\text{Li}\cdots\text{H}-\text{B}$ interaction appeared to be more pronounced than the corresponding intermolecular delocalization. We further noticed in $\text{LiN}(\text{CH}_3)_2\text{BH}_3$ that formation of intermolecular $\text{Li}\cdots\text{H}-\text{B}$ interactions enforces charge delocalization within the homopolar $\text{BH}\cdots\text{HB}$ contacts which explains the presence of the QTAIM bond critical points between clashing hydrogen atoms as was found by McGrady *et al.* [29]. In contrast, our investigations allowed us to conclude that monomers of $\text{LiN}(\text{CH}_3)_2\text{BH}_3$ are not likely to spontaneously form any stable aggregates via “pure” stabilizing $\text{BH}\cdots\text{HB}$ interactions (BH_3 to BH_3 orientation) due to the presence of negatively charged borane units—from a fundamental point of view it demonstrates that $\text{BH}\cdots\text{HB}$ interactions can be rather considered as destabilizing in this type of compounds. We further confirmed this conclusion by the Interacting Quantum Atoms (IQA) energy decomposition calculations—namely, the dihydrogen interaction energy in $\text{BH}\cdots\text{HB}$ appeared to be

significantly positive (destabilizing), $E_{\text{int}}^{\text{B(H)}\cdots\text{H(B)}} = +49.4$ kcal/mol as opposed to Li \cdots H–B interactions, $E_{\text{int}}^{\text{Li}\cdots\text{H(B)}} = -98.8$ kcal/mol.

Contrary to homopolar BH \cdots HB interactions, the ETS-NOCV and IQA methods allowed us to identify stabilizing homopolar dihydrogen interactions CH \cdots HC in both LiN(CH₃)₂BH₃ and KN(CH₃)₂BH₃—the presence of such stabilization has already been suggested by McGrady and coworkers based on a topological QTAIM study [29]. We found herein quantitatively that these interactions are dispersion dominated (64% for LiN(CH₃)₂BH₃ and 69% for KN(CH₃)₂BH₃), followed by charge transfer (13% for both LiN(CH₃)₂BH₃ and KN(CH₃)₂BH₃) and electrostatic (23% for LiN(CH₃)₂BH₃ and 17% for KN(CH₃)₂BH₃) terms. It was confirmed that these interactions are far stronger in the potassium crystal due to the larger number of CH \cdots HC contacts compared to the lithium analogue. Moreover, the NOCV-based deformation density contributions allowed to state that the “electronic” part of the CH \cdots HC interaction is based on both donation from the occupied $\sigma(\text{C-H})$ bonds into the empty $\sigma^*(\text{C-H})$ of methyl groups as well as polarization of the C–H bonds (mixing of $\sigma/\sigma^*(\text{C-H})$).

Briefly summarizing, our in-depth theoretical investigations performed by means of the ETS-NOCV and IQA energy decomposition methods, electrostatic potentials and charges, allowed us to confirm most of the findings that have been already reported in the pioneering work of McGrady *et al.* [29]. Furthermore, we provided for the first time the energetic description of non-covalent interactions contributing to the stability of LiNMe₂BH₃ and KNMe₂BH₃ as well demonstrating, contrary to McGrady *et al.* [29], the repulsive nature of the homopolar interactions BH \cdots HB. The latter is in line with numerous experimental papers [68–72]. Due to the fact that our calculations are based on the cluster approach as well as the fact that all theoretical methods are not free from approximations and very often not from arbitrariness, we believe that further works are needed from both theoretical and experimental laboratories in order to fully uncover the nature of homopolar BH \cdots HB interactions.

Supplementary Materials: The supplementary materials are available at <http://www.mdpi.com/2073-4352/6/3/28/s1>.

Acknowledgments: Results presented in this work were partially obtained using PL-Grid Infrastructure and resources provided by ACC Cyfronet AGH.

Author Contributions: Filip Sagan performed the majority of the calculations presented in this work. In addition, Filip Sagan contributed to the interpretation of the results and the final manuscript form. Radosław Filas initiated the work on bonding in LiN(CH₃)₂BH₃ and KN(CH₃)₂BH₃. Mariusz P. Mitoraj interpreted the results as well as writing the manuscript text.

Conflicts of Interest: The authors declare no conflict of interest.

References

1. Christopher, K.; Dimitrios, R. A review on energy comparison of hydrogen production methods from renewable energy sources. *Energy Environ. Sci.* **2012**, *5*, 6640–6651.
2. Dincer, I.; Acar, C. Review and evaluation of hydrogen production methods for better sustainability. *Int. J. Hydrog. Energy* **2015**, *40*, 11094–11111.
3. Dutta, S. A review on production, storage of hydrogen and its utilization as an energy resource. *J. Ind. Eng. Chem.* **2014**, *20*, 1148–1156.
4. Staubitz, A.; Robertson, A.P.M.; Manners, I. Ammonia-Borane and Related Compounds as Dihydrogen Sources. *Chem. Rev.* **2010**, *110*, 4079–4124.
5. Hamilton, C.W.; Baker, R.T.; Staubitz, A.; Manners, I. B–N compounds for chemical hydrogen storage. *Chem. Soc. Rev.* **2009**, *38*, 279–293.
6. Kim, S.-K.; Han, W.-S.; Kim, T.-J.; Kim, T.-Y.; Nam, S.W.; Mitoraj, M.; Piękoś, Ł.; Michalak, A.; Hwang, S.-J.; Kang, S.O. Palladium Catalysts for Dehydrogenation of Ammonia Borane with Preferential B–H Activation. *J. Am. Chem. Soc.* **2010**, *132*, 9954–9955.

7. Parafiniuk, M.; Mitoraj, M.P. Origin of Binding of Ammonia-Borane to Transition-Metal-Based Catalysts: An Insight from the Charge and Energy Decomposition Method ETS-NOCV. *Organometallics* **2013**, *32*, 4103–4113.
8. Parafiniuk, M.; Mitoraj, M.P. On the origin of internal rotation in ammonia borane. *J. Mol. Model.* **2014**, *20*, 2272–2281. [[CrossRef](#)] [[PubMed](#)]
9. Huang, Z.; Autrey, T. Boron–nitrogen–hydrogen (BNH) compounds: Recent developments in hydrogen storage, applications in hydrogenation and catalysis, and new syntheses. *Energy Environ. Sci.* **2012**, *5*, 9257–9268. [[CrossRef](#)]
10. Umegaki, T.; Yan, J.M.; Zhang, X.B.; Shioyama, H.; Kuriyama, N.; Xu, Q. Boron- and nitrogen-based chemical hydrogen storage materials. *Int. J. Hydrog. Energy* **2009**, *34*, 2303–2311. [[CrossRef](#)]
11. Custelcean, R.; Jackson, J.E. Dihydrogen Bonding: Structures, Energetics, and Dynamics. *Chem. Rev.* **2001**, *101*, 1963–1980. [[CrossRef](#)] [[PubMed](#)]
12. Bakmutov, V.I. *Dihydrogen Bonds: Principles, Experiments and Applications*; Wiley-Interscience: Hoboken, NJ, USA, 2008.
13. Mitoraj, M. Bonding in Ammonia Borane: An Analysis Based on the Natural Orbitals for Chemical Valence and the Extended Transition State Method (ETS-NOCV). *J. Phys. Chem. A* **2011**, *115*, 14708–14716. [[CrossRef](#)] [[PubMed](#)]
14. Jonas, V.; Frenking, G.; Reetz, M.T. Comparative Theoretical Study of Lewis Acid-Base Complexes of BH₃, BF₃, BCl₃, AlCl₃, and SO₂. *J. Am. Chem. Soc.* **1994**, *116*, 8741–8753. [[CrossRef](#)]
15. Merino, G.; Bakmutov, V.I.; Vela, A. Do Cooperative Proton-Hydride explain the Gas-Solid Structural Difference of BH₃NH₃? *J. Phys. Chem. A* **2002**, *106*, 8491–8994. [[CrossRef](#)]
16. Popelier, P.L.A. Characterization of a Dihydrogen Bond on the Basis of the Electron Density. *J. Phys. Chem. A* **1998**, *102*, 1873–1878. [[CrossRef](#)]
17. Wolstenholme, D.J.; Traboulee, K.T.; Hua, Y.; Calhoun, L.A.; McGrady, G.S. Thermal desorption of hydrogen from ammonia borane: Unexpected role of homopolar B–H ··· H–B interactions. *Chem. Commun.* **2012**, *48*, 2597–2599. [[CrossRef](#)] [[PubMed](#)]
18. Guerra, D.; David, J.; Restrepo, A. (H₃N–BH₃)₄: The ammonia borane tetramer. *Phys. Chem. Chem. Phys.* **2012**, *14*, 14892–14897. [[CrossRef](#)] [[PubMed](#)]
19. Chen, X.; Yuan, F.; Tan, Y.; Tang, Z.; Yu, X. Improved Dehydrogenation Properties of Ca(BH₄)₂ · nNH₃ (n = 1, 2, and 4) Combined with Mg(BH₄)₂. *J. Phys. Chem. C* **2012**, *116*, 21162–21168. [[CrossRef](#)]
20. Wolstenholme, D.J.; Dobson, J.L.; McGrady, G.S. Homopolar dihydrogen bonding in main group hydrides: Discovery, consequences, and applications. *Dalton Trans.* **2015**, *44*, 9718–9731.
21. Wolstenholme, D.J.; Fradsham, E.J.; McGrady, G.S. Supramolecular interactions in boron hydrides: How non-classical bonding directs their crystal architecture. *CrystEngComm* **2015**, *17*, 7623–7627. [[CrossRef](#)]
22. Chen, X.; Zhao, J.C.; Shore, S.G. The Roles of Dihydrogen Bonds in Amine Borane Chemistry. *Acc. Chem. Res.* **2013**, *46*, 2666–2675. [[CrossRef](#)] [[PubMed](#)]
23. Sagan, F.; Piękoś, Ł.; Andrzejak, M.; Mitoraj, M.P. From Saturated BN–compounds to Isoelectronic BN/CC Counterparts—An Insight from Computational Perspective. *Chemistry* **2015**, *21*, 15299–15307. [[CrossRef](#)] [[PubMed](#)]
24. Grochala, W.; Edwards, P.P. Thermal Decomposition of the Non-Interstitial Hydrides for the Storage and Production of Hydrogen. *Chem. Rev.* **2004**, *104*, 1283–1316. [[CrossRef](#)] [[PubMed](#)]
25. Dovgaliuk, I.; Le Duff, C.S.; Robeyns, K.; Devillers, M.; Filinchuk, Y. Mild Dehydrogenation of Ammonia Borane Complexed with Aluminum Borohydride. *Chem. Mater.* **2015**, *27*, 768–777. [[CrossRef](#)]
26. Orimo, S.; Nakamori, Y.; Eliseo, J.R.; Züttel, A.; Jensen, C.M. Complex Hydrides for Hydrogen Storage. *Chem. Rev.* **2007**, *107*, 4111–4132. [[CrossRef](#)] [[PubMed](#)]
27. Luoa, J.; Wub, H.; Zhou, W.; Kang, X.; Fang, Z.; Wang, P. LiBH₄ · NH₃BH₃: A new lithium borohydride ammonia borane compound with a novel structure and favorable hydrogen storage properties. *Int. J. Hydrog. Energy* **2012**, *37*, 10750–10757. [[CrossRef](#)]
28. Jaroń, T.; Orłowski, P.A.; Wegner, W.; Fijałkowski, K.J.; Leszczyński, P.J.; Grochala, W. Hydrogen Storage Materials: Room-Temperature Wet-Chemistry Approach toward Mixed-Metal Borohydrides. *Angew. Chem. Int. Ed.* **2015**, *54*, 1236–1239. [[CrossRef](#)] [[PubMed](#)]
29. Wolstenholme, D.J.; Flogeras, J.; Che, F.N.; Decken, A.; McGrady, G.S. Homopolar Dihydrogen Bonding in Alkali Metal Amidoboranes: Crystal Engineering of Low-Dimensional Molecular Materials. *J. Am. Chem. Soc.* **2013**, *135*, 2439–2442. [[CrossRef](#)] [[PubMed](#)]

30. Bader, R.F.W. *Atoms in Molecules: A Quantum Theory*; Oxford University Press: Oxford, UK, 1990.
31. Weinhold, F.; Schleyer, P.R.; McKee, W.C. Bay-Type H–H “Bonding” in cis-2-Butene and Related Species: QTAIM Versus NBO Description. *J. Computat. Chem.* **2014**, *35*, 1499–1508. [[CrossRef](#)] [[PubMed](#)]
32. Poater, J.; Solà, M.; Bickelhaupt, F.M. Hydrogen–Hydrogen Bonding in Planar Biphenyl, Predicted by Atoms-In-Molecules Theory, Does Not Exist. *Chemistry* **2006**, *12*, 2889–2895. [[CrossRef](#)] [[PubMed](#)]
33. Grimme, S.; Mück-Lichtenfeld, C.; Erker, G.; Kehr, G.; Wang, H.; Beckers, H.; Willner, H. When Do Interacting Atoms Form a Chemical Bond? Spectroscopic Measurements and Theoretical Analyses of Dideuteriophenanthrene. *Angew. Chem. Int. Ed.* **2009**, *48*, 2592–2595. [[CrossRef](#)] [[PubMed](#)]
34. Jacobsen, H. Kinetic energy density and covalent bonding—A complementary analysis at the border of bond and no bond. *Dalton Trans.* **2010**, *39*, 5426–5428. [[CrossRef](#)] [[PubMed](#)]
35. Hancock, R.D.; Nikolayenko, I.V. Do Nonbonded H–H Interactions in Phenanthrene Stabilize It Relative to Anthracene? A Possible Resolution to this Question and Its Implications for Ligands such as 2,2′-Bipyridyl. *J. Phys. Chem. A* **2012**, *116*, 8572–8583. [[CrossRef](#)] [[PubMed](#)]
36. Cukrowski, I.; de Lange, J.H.; Adeyinka, A.S.; Mangondo, P. Evaluating common QTAIM and NCI interpretations of the electron density concentration through IQA interaction energies and 1D cross-sections of the electron and deformation density distributions. *Comput. Theor. Chem.* **2015**, *1053*, 60–76. [[CrossRef](#)]
37. Safin, D.A.; Babashkina, M.G.; Robeyns, K.; Mitoraj, M.P.; Kubisiak, P.; Garcia, Y. Influence of the Homopolar Dihydrogen Bonding CH ··· HC on Coordination Geometry: Experimental and Theoretical Studies. *Chemistry* **2015**, *21*, 16679–16687. [[CrossRef](#)] [[PubMed](#)]
38. Cukrowski, I. IQA-embedded fragment attributed molecular system energy change in exploring intramolecular interactions. *Comput. Theor. Chem.* **2015**, *1066*, 62–75. [[CrossRef](#)]
39. Cukrowski, I.; Govender, K.K.; Mitoraj, M.P.; Srebro, M. QTAIM and ETS-NOCV Analyses of Intramolecular CH ··· HC Interactions in Metal Complexes. *J. Phys. Chem. A* **2011**, *115*, 12746–12757. [[CrossRef](#)] [[PubMed](#)]
40. Cukrowski, I.; de Lange, J.H.; Mitoraj, M.P. Physical Nature of Interactions in ZnII Complexes with 2,2′-Bipyridyl: Quantum Theory of Atoms in Molecules (QTAIM), Interacting Quantum Atoms (IQA), Noncovalent Interactions (NCI), and Extended Transition State Coupled with Natural Orbitals for Chemical Valence (ETS-NOCV) Comparative Studies. *J. Phys. Chem. A* **2014**, *118*, 623–637. [[PubMed](#)]
41. Safin, D.A.; Babashkina, M.G.; Kubisiak, P.; Mitoraj, M.P.; Le Duff, C.S.; Robeyns, K.; Garcia, Y. Crucial influence of the intramolecular hydrogen bond on the coordination mode of RC(S)NHP(S)(OiPr)₂ in homoleptic complexes with Ni^{II}. *Eur. J. Inorg. Chem.* **2013**, *2013*, 545–555.
42. Lyngvi, E.; Sanhueza, I.A.; Schoenebeck, F. Dispersion Makes the Difference: Bisligated Transition States Found for the Oxidative Addition of Pd(PtBu₃)₂ to Ar-OSO₂R and Dispersion-Controlled Chemoselectivity in Reactions with Pd[P(iPr)(tBu)₂]₂. *Organometallics* **2015**, *34*, 805–812. [[CrossRef](#)]
43. Wolters, L.P.; Koekkoek, R.; Bickelhaupt, F.M. Role of Steric Attraction and Bite-Angle Flexibility in Metal-Mediated C–H Bond Activation. *ACS Catal.* **2015**, *5*, 5766–5775. [[CrossRef](#)]
44. Bader, R.F.W. Pauli Repulsions Exist Only in the Eye of the Beholder. *Chemistry* **2006**, *12*, 2896–2901. [[CrossRef](#)] [[PubMed](#)]
45. Hernández-Trujillo, J.; Matta, C.F. Hydrogen–hydrogen bonding in biphenyl revisited. *Struct. Chem.* **2007**, *18*, 849–857. [[CrossRef](#)]
46. Matta, C.F.; Sadjadi, S.A.; Braden, D.A.; Frenking, G. The Barrier to the Methyl Rotation in Cis-2-Butene and its Isomerization Energy to Trans-2-Butene, Revisited. *J. Comput. Chem.* **2016**, *37*, 143–154. [[CrossRef](#)] [[PubMed](#)]
47. Mitoraj, M.P.; Michalak, A. Natural orbitals for chemical valence as descriptors of chemical bonding in transition metal complexes. *J. Mol. Model.* **2007**, *13*, 347–355. [[CrossRef](#)] [[PubMed](#)]
48. Michalak, A.; Mitoraj, M.P.; Ziegler, T. Bond Orbitals from Chemical Valence Theory. *J. Phys. Chem. A* **2008**, *112*, 1933–1939. [[CrossRef](#)] [[PubMed](#)]
49. Mitoraj, M.P.; Michalak, A.; Ziegler, T. A Combined Charge and Energy Decomposition Scheme for Bond Analysis. *J. Chem. Theory Comput.* **2009**, *5*, 962–975. [[CrossRef](#)] [[PubMed](#)]
50. Mitoraj, M.P.; Michalak, A. Theoretical description of halogen bonding—An insight based on the natural orbitals for chemical valence combined with the extended-transition-state method (ETS-NOCV). *J. Mol. Model.* **2013**, *19*, 4681–4688. [[CrossRef](#)] [[PubMed](#)]

51. Mitoraj, M.P.; Janjic, G.V.; Medakovic, V.B.; Veljkovic, D.Z.; Michalak, A.; Zaric, S.D.; Milcic, M.K. Nature of the Water/Aromatic Parallel Alignment Interactions. *J. Comput. Chem.* **2015**, *36*, 171–180. [[CrossRef](#)] [[PubMed](#)]
52. Te Velde, G.; Bickelhaupt, F.M.; Baerends, E.J.; Fonseca Guerra, C.; van Gisbergen, S.J.A.; Snijders, J.G.; Ziegler, T. Chemistry with ADF. *J. Comput. Chem.* **2001**, *22*, 931–967. [[CrossRef](#)]
53. Bickelhaupt, F.M.; Baerends, E.J. Kohn-Sham Density Functional Theory: Predicting and Understanding Chemistry. *Rev. Comput. Chem.* **2007**, *15*, 1–86.
54. Baerends, E.J.; Autschbach, J.; Bashford, D.; Bérces, A.; Bickelhaupt, F.M.; Bo, C.; Boerrigter, P.M.; Cavallo, L.; Chong, D.P.; Deng, L.; *et al.* *SCM Theoretical Chemistry*; ADF2012.01; Vrije Universiteit: Amsterdam, The Netherlands, 2012.
55. Johnson, E.R.; Keinan, S.; Mori-Sánchez, P.; Contreras-García, J.; Cohen, A.J.; Yang, W. Revealing Noncovalent Interactions. *J. Am. Chem. Soc.* **2010**, *132*, 6498–6506. [[CrossRef](#)] [[PubMed](#)]
56. Blanco, M.A.; Pendás, A.M.; Francisco, E. Interacting Quantum Atoms: A Correlated Energy Decomposition Scheme Based on the Quantum Theory of Atoms in Molecules. *J. Chem. Theory Comput.* **2005**, *1*, 1096–1109. [[CrossRef](#)] [[PubMed](#)]
57. Gao, W.; Feng, H.; Xuan, X.; Chen, L. The assessment and application of an approach to noncovalent interactions: The energy decomposition analysis (EDA) in combination with DFT of revised dispersion correction (DFT-D3) with Slater-type orbital (STO) basis set. *J. Mol. Model.* **2012**, *18*, 4577–4589. [[CrossRef](#)] [[PubMed](#)]
58. Van der Wijst, T.; Fonseca Guerra, C.; Swart, M.; Bickelhaupt, F.M.; Lippert, B. A Ditopic Ion-Pair Receptor Based on Stacked Nucleobase Quartets. *Angew. Chem. Int. Ed.* **2009**, *48*, 3285–3287. [[CrossRef](#)] [[PubMed](#)]
59. Fonseca Guerra, C.; van der Wijst, T.; Poater, J.; Swart, M.; Bickelhaupt, F.M. Adenine *versus* guanine quartets in aqueous solution: Dispersion-corrected DFT study on the differences in *p*-stacking and hydrogen-bonding behavior. *Theor. Chem. Acc.* **2010**, *125*, 245–252. [[CrossRef](#)]
60. Grimme, S. Semiempirical GGA-Type Density Functional Constructed with a Long-Range Dispersion Correction. *J. Comput. Chem.* **2006**, *27*, 1787–1799. [[CrossRef](#)] [[PubMed](#)]
61. Frisch, M.J.; Trucks, G.W.; Schlegel, H.B.; Scuseria, G.E.; Robb, M.A.; Cheeseman, J.R.; Scalmani, G.; Barone, V.; Mennucci, B.; Petersson, G.A.; *et al.* *Gaussian 09*; Gaussian Inc.: Wallingford, CT, USA, 2009.
62. Ziegler, T.; Rauk, A. On the calculation of bonding energies by the Hartree Fock Slater method. *Theor. Chim. Acta* **1977**, *46*, 1–10. [[CrossRef](#)]
63. AIMAll, Version 13.05.06 Professional. Todd A. Keith, TK Gristmill Software, Overland Park, KS, USA, 2016.
64. Politzer, P.; Murray, J.S.; Clark, T. Halogen bonding: An electrostatically-driven highly directional noncovalent interaction. *Phys. Chem. Chem. Phys.* **2010**, *12*, 7748–7757. [[CrossRef](#)] [[PubMed](#)]
65. Politzer, P.; Murray, J.S.; Janjić, G.V.; Zarić, S.D. σ -Hole Interactions of Covalently-Bonded Nitrogen, Phosphorus and Arsenic: A Survey of Crystal Structures. *Crystals* **2014**, *4*, 12–31. [[CrossRef](#)]
66. Clark, T.; Murray, J.S.; Politzer, P. The Role of Polarization in a Halogen Bond. *Aust. J. Chem.* **2014**, *67*, 451–456. [[CrossRef](#)]
67. Politzer, P.; Murray, J.S.; Clark, T. Mathematical modeling and physical reality in noncovalent interactions. *J. Mol. Model.* **2015**, *52*, 21–31. [[CrossRef](#)] [[PubMed](#)]
68. Schouwink, P.; Hagemann, H.; Embs, J.P.; Anna, V.D.; Černý, R. Di-hydrogen contact induced lattice instabilities and structural dynamics in complex hydride perovskites. *J. Phys. Condens. Matter* **2015**, *27*, 265403–265415. [[CrossRef](#)] [[PubMed](#)]
69. Černý, R.; Kim, K.C.; Penin, N.; D’Anna, V.; Hagemann, H.; Sholl, D.S. AZn₂(BH₄)₅ (A = Li, Na) and NaZn(BH₄)₃: Structural Studies. *J. Phys. Chem. C* **2010**, *114*, 19127–19133. [[CrossRef](#)]
70. Černý, R.; Ravnsbæk, D.B.; Schouwink, P.; Filinchuk, Y.; Penin, N.; Teyssier, J.; Smrčok, L.; Jensen, T.R. Potassium Zinc Borohydrides Containing Triangular [Zn(BH₄)₃] and Tetrahedral [Zn(BH₄)Cl₄]₂ Anions. *J. Phys. Chem. C* **2012**, *116*, 1563–1571. [[CrossRef](#)]
71. Ravindran, P.; Vajeeston, P.; Vidya, R.; Kjekshus, A.; Fjellvåg, H. Violation of the Minimum H–H Separation “Rule” for Metal Hydrides. *Phys. Rev. Lett.* **2002**, *89*, 106403–106407.
72. Ravnsbæk, D.; Filinchuk, Y.; Cerenius, Y.; Jakobsen, H.J.; Besenbacher, F.; Skibsted, J.; Jensen, T.R. A Series of Mixed-Metal Borohydrides. *Angew. Chem. Int. Ed.* **2009**, *48*, 6659–6663.

73. Demyanov, P.; Polestshuk, P. A Bond Path and an Attractive Ehrenfest Force Do Not Necessarily Indicate Bonding Interactions: Case Study on M_2X_2 ($M = Li, Na, K; X = H, OH, F, Cl$). *Chemistry* **2012**, *18*, 4982–4993. [[CrossRef](#)] [[PubMed](#)]
74. Wang, C.; Danovich, D.; Mo, Y.; Shaik, S. On The Nature of the Halogen Bond. *J. Chem. Theory Comput.* **2014**, *10*, 3726–3737. [[CrossRef](#)] [[PubMed](#)]
75. Grabowski, S.J. Hydrogen and Halogen Bonds Are Ruled by the Same Mechanisms. *Phys. Chem. Chem. Phys.* **2013**, *15*, 7249–7259. [[CrossRef](#)] [[PubMed](#)]
76. Mulliken, R.S. Structures of Complexes Formed by Halogen Molecules with Aromatic and with Oxygenated Solvents. *J. Am. Chem. Soc.* **1950**, *72*, 600–608. [[CrossRef](#)]
77. Echeverría, J.; Aullón, G.; Danovich, D.; Shaik, S.; Alvarez, S. Dihydrogen contacts in alkanes are subtle but not faint. *Nat. Chem.* **2011**, *3*, 323–330. [[CrossRef](#)] [[PubMed](#)]
78. Danovich, D.; Shaik, S.; Neese, F.; Echeverría, J.; Aullón, G.; Alvarez, S. Understanding the Nature of the $CH \cdots HC$ Interactions in Alkanes. *J. Chem. Theory Comput.* **2013**, *9*, 1977–1991. [[CrossRef](#)] [[PubMed](#)]
79. Grimme, S.; Schreiner, P.R. Steric Crowding Can Stabilize a Labile Molecule: Solving the Hexaphenylethane Riddle. *Angew. Chem. Int. Ed.* **2011**, *50*, 12639–12642. [[CrossRef](#)] [[PubMed](#)]
80. Fokin, A.; Chernish, L.V.; Gunchenko, P.A.; Tikhonchuk, E.Y.; Hausmann, H.; Serafin, M.; Dahl, J.E.P.; Carlson, R.M.K.; Schreiner, P.R. Stable Alkanes Containing Very Long Carbon–Carbon Bonds. *J. Am. Chem. Soc.* **2012**, *134*, 13641–13650. [[CrossRef](#)] [[PubMed](#)]
81. Zhang, J.; Dolg, M. Dispersion Interaction Stabilizes Sterically Hindered Double Fullerenes. *Chemistry* **2014**, *20*, 13909–13912. [[CrossRef](#)] [[PubMed](#)]
82. Grabowski, S.J.; Pfitzner, A.; Zabel, M.; Dubis, A.T.; Palusiak, M. Intramolecular $H \cdots H$ Interactions for the Crystal Structures of [4-((E)-But-1-enyl)-2,6-dimethoxyphenyl] pyridine-3-carboxylate and [4-((E)-Pent-1-enyl)-2,6-dimethoxyphenyl] pyridine-3-carboxylate; DFT Calculations on Modeled Styrene Derivatives. *J. Phys. Chem. B* **2004**, *108*, 1831–1837. [[CrossRef](#)]
83. Grabowski, S.J. Dihydrogen bond and $X-H \cdots \sigma$ interaction as sub-classes of hydrogen bond. *J. Phys. Org. Chem.* **2013**, *26*, 452–459. [[CrossRef](#)]
84. Grabowski, S.J.; Sokalski, W.A.; Leszczynski, J. Nature of $X-H^{+\delta} \cdots -\delta H-Y$ dihydrogen bonds and $X-H \cdots \sigma$ Interactions. *J. Phys. Chem. A* **2004**, *108*, 5823–5830. [[CrossRef](#)]
85. Grabowski, S.J.; Sokalski, W.A.; Leszczynski, J. How short can the $H \cdots H$ intermolecular contact can be? New findings that reveal the covalent nature of extremely strong interactions. *J. Phys. Chem. A* **2005**, *109*, 4331–4341. [[CrossRef](#)] [[PubMed](#)]
86. Krapp, A.; Frenking, G.; Uggerud, E. Nonpolar Dihydrogen Bonds—On a Gliding Scale from Weak Dihydrogen Interaction to Covalent H–H in Symmetric Radical Cations $[H_n E-H-H-EH_n]^+$. *Chemistry* **2008**, *14*, 4028–4038. [[CrossRef](#)] [[PubMed](#)]
87. Kim, D.Y.; Singh, N.J.; Lee, H.M.; Kim, K.S. Hydrogen-Release Mechanisms in Lithium Amidoboranes. *Chemistry* **2009**, *15*, 5598–5604. [[CrossRef](#)] [[PubMed](#)]
88. Lee, T.B.; McKee, M.L. Mechanistic Study of $LiNH_2BH_3$ Formation from $(LiH)_4 + NH_3BH_3$ and Subsequent Dehydrogenation. *Inorg. Chem.* **2009**, *48*, 7564–7575. [[CrossRef](#)] [[PubMed](#)]
89. Luedtke, A.T.; Autrey, T. Hydrogen Release Studies of Alkali Metal Amidoboranes. *Inorg. Chem.* **2010**, *49*, 3905–3910. [[CrossRef](#)] [[PubMed](#)]

